Regular Article - Theoretical Physics

Resolved photons in SHERPA

Stefan Höche[1,a], **Frank Krauss**[2,b], **Peter Meinzinger**[2,c]

[1] Fermi National Accelerator Laboratory, Batavia, IL 60510, USA
[2] Institute for Particle Physics Phenomenology, Durham University, Durham DH1 3LE, UK

© The Author(s) 2024

Abstract We present the first complete simulation framework, in the SHERPA event generator, for resolved photon interactions at next-to leading order accuracy. It includes photon spectra obtained through the equivalent-photon approximation, parton distribution functions to parametrize the hadronic structure of quasi-real photons, the matching of the parton shower to next-to leading order QCD calculations for resolved photon cross sections, and the modelling of multiple-parton interactions. We validate our framework against a wide range of photo-production data from LEP and HERA experiments, observing good overall agreement. We identify important future steps relevant for high-quality simulations at the planned Electron–Ion Collider.

1 Introduction

Photon-induced processes provide a rich testing ground for a wide range of physics effects. This is, on one hand, because photons will couple to any electromagnetically charged particle, resulting in a wide spectrum of accessible final states. On the other hand, photons have the quantum numbers of (neutral vector) mesons and their wave functions therefore have a sizeable hadronic component which lets them interact strongly, with correspondingly large cross sections. The production of low–multiplicity final states in $\gamma\gamma$ collisions has been observed in many experiments [1–4], and yields interesting insights into the physics of hadrons and hadron resonances described by effective theories of the strong interactions. At increasing centre-of-mass energies of the colliding photons, new channels open up, and the production of jets has been studied, for example, at LEP [5–10]. Similarly,

the photo–production of various final states, including jets, has been analysed by the HERA experiments [11–17].

The results obtained in these experiments have allowed to parameterise the parton content of the hadronic component of quasi-real photons in the form of parton distribution functions (PDFs), for example in the GRV [18], CJK [19,20], SAL [21], and SaS [22,23] sets.[1] In fact, based on these PDFs, satisfying agreement between data and calculations has been achieved, and a complete model for photon structure functions and high–energy photon interactions [24] has been encoded in PYTHIA [25]. There, the hard production of QCD final states at large scales, *i.e.* jets, is simulated in the usual way by dressing the hard parton–level matrix element with subsequent parton showers, the fragmentation of the resulting partons into hadrons during hadronization, possibly including an underlying event. Recently, the model was extended to also include the perpendicular component of the photon momentum [26].

Pushing for higher accuracy, there have been a few predictions for inclusive jet-production at fixed-order at HERA [27–31] and the EIC [32], while more attention has recently been paid to exclusive meson production processes and photoproduction at heavy-ion collisions [33–38].

[a] e-mail: shoeche@fnal.gov

[b] e-mail: frank.krauss@durham.ac.uk

[c] e-mail: peter.meinzinger@durham.ac.uk (corresponding author)

---

[1] To fix the (non–perturbative) inputs for the PDFs at some infrared scale $Q_0^2 \approx \mathcal{O}(1\,\mathrm{GeV}^2)$ different ansätze have been chosen. Most of them rely on the vector meson dominance model which assumes that at these scales the hadronic component of the photon wave function behaves like a vector meson, and use the pion PDF with modifications inspired by the quark model. The more involved SaS model for the photon structure function is based on the decomposition of the photon wave function $|\gamma\rangle$ into three components: a "bare" photon component $|\gamma_{\mathrm{bare}}\rangle$ where the photon interacts indeed as a point–particle, a non–perturbative component $|\gamma_V\rangle$ where the photon fluctuates into various neutral vector mesons V such as ρ, ω, ϕ, J/ψ *etc.*, and a perturbative "anomalous component" $|\gamma_{q\bar{q}}\rangle$ in which the photon fluctuates into a $q\bar{q}$ pair. In all cases, the PDF at the low scale Q_0^2 is translated to PDFs at larger scales through standard QCD evolution, by emitting secondary virtual partons.

Anticipating the increased precision requirements for successfully operating a possible future lepton collider such as FCC-ee or the planned electron–ion collider, EIC, motivates to revisit the physics of photon–induced processes and to arrive at fully-differential predictions at Next-To-Leading Order (NLO) in QCD perturbation theory. We report here on the systematic inclusion of PDFs for quasi–real photons into the SHERPA event generation framework [39,40], the modelling of multiple-parton interactions, and the extension of the calculation to Next-to-Leading Order matched to the parton shower. The paper is organised as follows. In Sect. 2 we briefly discuss how SHERPA combines the equivalent photon approximation (EPA) and photon PDFs, with some emphasis on the efficient integration over the resulting phase space, the matching to the parton shower at NLO and the multiple-parton interactions (MPI) model. In Sect. 3 we will show some first results of full Monte Carlo simulations, comparing results obtained with SHERPA to data from both the LEP and HERA experiments at MC@NLO accuracy. We present comparisons to Leading Order and study the effect of the MPI. We summarise our findings in Sect. 4.

2 Equivalent photons and their PDFs

For the simulation of photo-production events in SHERPA, we use its existing EPA interface, improved the phase space handling for the initial states for a more efficient integration, and added relevant photon PDFs to SHERPA's internal PDF interface. The resulting code will be publically available as part of the upcoming release of SHERPA 3.0; in the meantime it can be obtained from the authors upon request.

2.1 Phase space handling

In the following we detail the structures for efficient phase space sampling, using the most involved example of doubly resolved photon–photon collisions at lepton colliders, schematically depicted in Fig. 1; the cases of direct pho-

tons, the corresponding ISR terms do not need to be taken into account and the corresponding phase space integration is simplified.

The two incoming leptons have momenta p_1 and p_2, and a (beam) c.m.-system characterised by the c.m.-energy squared s_{12} and its rapidity y_{12} in the lab system. The momenta of the photons emitted by the leptons, p_1' and p_2', create a (photon) c.m.-system characterised by its c.m.-energy squared s_{12}' and rapidity y_{12}' with respect to the beam system. The partonic structure of the photons, as described by the PDFs, results in two partons with momenta p_1'' and p_2'' to finally enter the hard process which will result in final state particles with momenta q_i''. The hard scattering is characterised by a c.m.-energy of s_{12}'' and a rapidity y_{12}'' w.r.t. the photon system. This structure requires two nested integrations for the two successive "initial states" (photons and partons): first an integration over s_{12}' and y_{12}', with factors given by the EPA spectra, and then an integration over s_{12}'' and y_{12}'', with factors given by the PDFs, before adding the integration over the final state phase space over the outgoing momenta q_i''. Efficient integration over this complex phase space in SHERPA is facilitated through the multi-channel method [41] with automatically generated integration channels that map out intrinsic structures such as s-channel resonances *etc.*

After the successful generation of a phase space point, the corresponding weight is calculated, given by the factors stemming from the EPA photon spectra and the PDF weights.

2.2 Equivalent photon approximation

The equivalent photon approximation encoded in the Weizsäcker-Williams formula [42–44] is based on the observation that quasi-virtual photons can be approximated through real photons for small virtualities $Q^2 < \Lambda_{cut}^2$. As photo-production events are dominated by the interaction of low-virtuality photons, the differential cross-section can be substituted by $d\sigma_{eX} = \sigma_{\gamma X}(Q^2 = 0)dn$. SHERPA uses an improved version of the spectrum, following [45], which introduces the term proportional to m_e^2 to the spectrum, and the photons are

Fig. 1 Schematic sketch of the phase space mappings between the different steps in the initial states, *i.e.* the Equivalent Photon Approximation (EPA) and the Initial State Radiation (ISR), and the Matrix Element (ME). Each coordinates pair of Mandelstam-$s^{\prime(\prime)}$ and rapidity $y^{\prime(\prime)}$ is randomly sampled and the momenta are calculated as functions of these
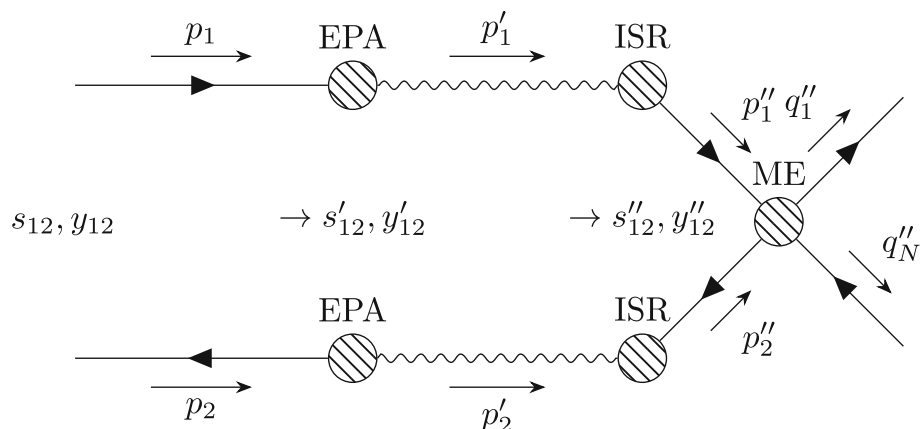
Table 1 Photon PDF libraries included in SHERPA and their properties

Name	# Sets	Virtual?	NLO?	# Flavours	x-range	μ_F^2-range
GRV [18]	2	No	Yes	5	$[10^{-5}, 1]$	$[0.25, 10^6]$
SAL [21]	1	No	Yes	6	$[10^{-5}, 0.9999]$	$[2, 8 \cdot 10^4]$
SaS [22,23]	4	Yes	Yes	6	$[10^{-5}, 1]$	$[0.25, 10^6]$
CJK [19,20]	4	No	Yes	5	$[10^{-5}, 1]$	$[0.25, 2 \cdot 10^5]$

assumed to be collinear to the electron beam. The dependence of the photon spectrum on the photon virtuality is integrated out. This results in the following spectrum for electrons:

$$
\mathrm{d}n = \frac{\alpha_{\mathrm{em}}}{2\pi} \frac{\mathrm{d}x}{x} \left[\left(1 + (1-x)^2 \right) \log \left(\frac{Q_{\mathrm{max}}^2}{Q_{\mathrm{min}}^2} \right) \right.
$$
$$
\left. - 2m_e^2 x^2 \left(\frac{1}{Q_{\mathrm{min}}^2} - \frac{1}{Q_{\mathrm{max}}^2} \right) \right] \tag{1}
$$

Here, x denotes the ratio of photon to electron energy, $\frac{E_\gamma}{E_e}$, and α_{em} is the electromagnetic coupling constant. Q_{max}^2 and Q_{min}^2 denote the maximal and minimal photon virtuality, where the latter can be calculated from kinematic restrictions and is given by

$$
Q_{\mathrm{min}}^2 = \frac{m_e^2 x^2}{1-x} . \tag{2}
$$

The maximal virtuality is given by the experimental setup and the maximal deflection angle of the electron, θ_{max}, below which the hard process is still considered to be photon-induced. It is given by

$$
Q_{\mathrm{max}}^2 = \min \left(Q_{\mathrm{min}}^2 + E_e^2 (1-x) \theta_{\mathrm{max}}^2, \ Q_{\mathrm{max,fixed}}^2 \right). \tag{3}
$$

Default choices are $\theta_{\mathrm{max}} = 0.3$ and $Q_{\mathrm{max,fixed}}^2 = 3\,\mathrm{GeV}^2$, but they can be overwritten by the user, cf. the SHERPA manual [46].

2.3 Photon PDFs

To facilitate a comparison over different parameterisations, four PDF libraries have been included in SHERPA, see Table 1 for a summary.

Currently, all PDFs are evaluated at virtuality $Q^2 = 0$; the extension to virtual photons, taking also into account longitudinal polarisations, will be introduced in a later release. The extraction of a parton from the photon is complemented by the corresponding treatment of the remaining partons. For this a similar procedure is applied as in the remnant construction for a hadron, however, with a few simplifications. As there are no valence quarks present in the photon, the remnant is constructed as the anti-particle of the hard-scattering quark. In the case of the gluons, a quark-antiquark pair is constructed from one of the light quark generations. In the

following processing, the photon remnants is treated analogously to a hadron remnant, *i.e.* its longitudinal momentum is distributed among the partons according to the kinematics, and their transverse momenta, given by some non-perturbative intrinsic k_T distribution, compensate each other.

2.4 NLO and matching to the parton shower

The procedure for a NLO calculation in photo-production has been presented in [47]. We will follow the same line of arguments for the matching to the parton shower, summarising the procedure in the following paragraphs. In contrast to the more familar case of hadronic PDFs, the evolution in the photon PDFs has an additional "source" term, related to the photon splitting into a quark–anti-quark pair, which is proportional to α_{em}. This means that the evolution of the parton distributions $f_i^{(\gamma)}$ for parton i in the photon follow [47]

$$
\frac{\partial f_i^{(\gamma)}}{\partial \log \mu^2} = \frac{\alpha_{\mathrm{em}}}{2\pi} P_{i\gamma} + \frac{\alpha_S}{2\pi} \sum_j P_{ij} \otimes f_j^{(\gamma)} . \tag{4}
$$

The first term on the r.h.s. of the equation above gives rise to the "anomalous component" mentioned before.

At Next-to-Leading-Order, there will be additional collinear divergences in the real-corrections, stemming from the photon splitting. These divergences appear only in the direct-photon component, but they can be subtracted using the splitting kernel from the corresponding term in the photon PDF evolution.

To ensure an exact cancellation between these terms, the PDF has to use the same factorisation scheme as the subtraction scheme, which in the case of SHERPA is the $\overline{\mathrm{MS}}$ scheme. This reduces the number of possible PDFs sets directly available for the NLO calculation in SHERPA down to SAS1M and SAS2M from the SaS library. We note that additional PDFs can be made available easily by adding the respective factorization scheme dependent correction terms [48]. Apart from this subtlety in the choice of PDFs both NLO calculations and full simulations proceed in full analogy to the more familiar case of, e.g., proton–proton collisions.
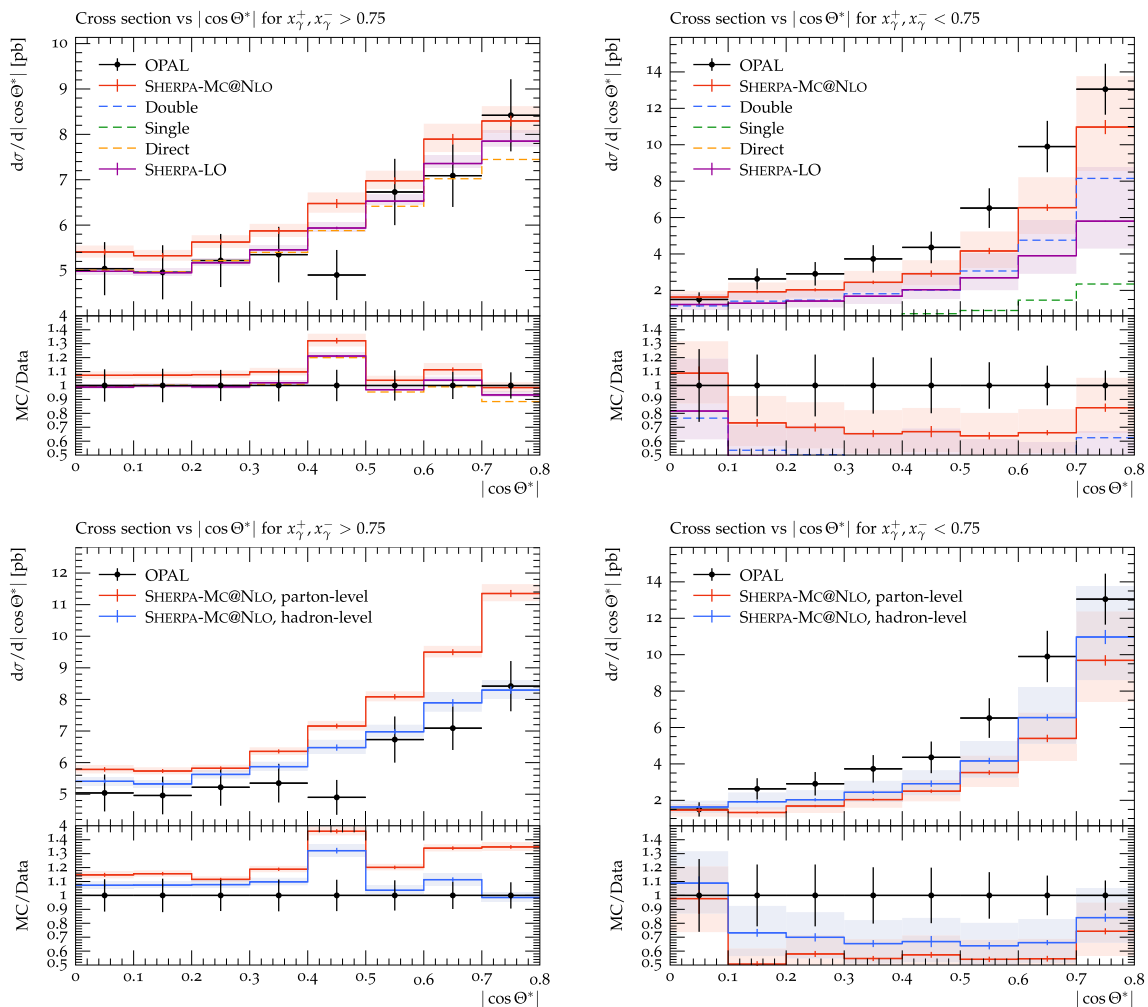
Fig. 2 Differential dijet inclusive cross section with respect to $\cos\theta^*$, defined in Eq. (9), comparing results of our SHERPA MC@NLO simulation at hadron-level with the LO simulation (top row) and with simulations at parton-level (bottom row) and with data from OPAL at an $e^- e^+$ c.m.-energy of 198 GeV [5]. In the left and right panels the requirement $x_\gamma^\pm < 0.75$ and $x_\gamma^\pm > 0.75$ are applied and enhance resolved and direct contributions, respectively

3 Validation of the framework

We will now turn to the validation of our implementation, comparing results at MC@NLO precision with photoproduction data from the OPAL and ZEUS experiments. For each collider set-up and energy we generated samples of $5 \cdot 10^6$ events per component at MC@NLO accuracy. For the calculation of matrix elements we used AMEGIC [49] and COMIX [50] for the tree-level matrix elements and subtraction terms [51] and OPENLOOPS [52] for the one-loop matrix elements. We added the CSSHOWER parton shower [53] for the jet evolution, matched with the MC@NLO method [54,55] as implemented in SHERPA [56]. Underlying event effects have been included through an implementation of the Sjostrand-

van Zijl model [57,58] within SHERPA,[2] and the partons were hadronized with the cluster fragmentation of AHADIC [59]. We consistently used the current default value for $\alpha_S = 0.118$ with three-loop running. As described in 2.4, the event generation must currently use PDFs based on the $\overline{\text{MS}}$ scheme, so the resolved-photon predictions were generated with, and averaged over, the SAS1M and SAS2M PDF sets. The factorisation scale and the renormalisation scale were both set to $\mu_F = \mu_R = H_T/2$ and we kept the 7-point variation for the scale uncertainty estimate.

We used the RIVET [60] framework with the existing analyses implementing [5–7,11,12]. For each experiment, different components of the cross-section have to be summed over,

---

[2] For details and a future tune to data we refer the reader to a forthcoming SHERPA manual.
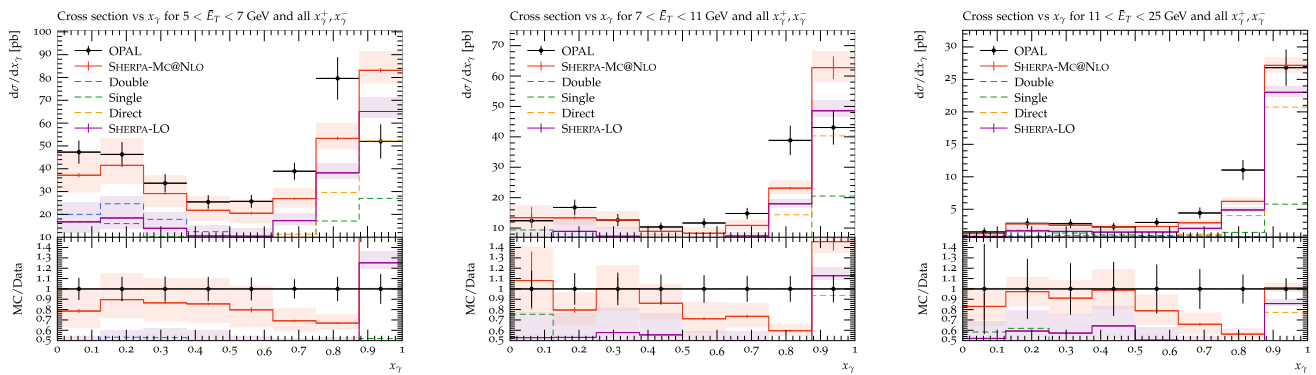
Fig. 3 Distributions $x_\gamma^\pm$, collectively denoted as x_γ, in different bins of average transverse jet energy: $\bar{E}_T \in [5\,\text{GeV}, 7\,\text{GeV}]$ (left), $\bar{E}_T \in [7\,\text{GeV}, 11\,\text{GeV}]$ (middle), $\bar{E}_T \in [11\,\text{GeV}, 25\,\text{GeV}]$ (right). Results of the SHERPA simulation with MC@NLO accuracy are compared with results at LO and with data from OPAL at an e^-e^+ c.m.-energy of 198 GeV [5]

for example,

$$\sigma_{\text{tot}} = \sigma_{\gamma\gamma} + \sigma_{j\gamma} + \sigma_{\gamma j} + \sigma_{jj} \tag{5}$$

for LEP and

$$\sigma_{\text{tot}} = \sigma_{\gamma j} + \sigma_{jj} \tag{6}$$

for HERA, where in both cases j denotes a photon or proton resolved through a PDF.

3.1 Comparison with LEP data

The OPAL analysis of photon-induced di-jet production at 198 GeV c.m.-energy [5] offers the most differential observables, and we use it as the primary reference for our validation of photo-production at LEP 2. To comply with experimental cuts, the k_T algorithm with a jet radius of $R = 1.0$ is used and cuts of $E_T > 4.5$ (2.5) GeV for the leading (subleading) jet are imposed.

$$x_\gamma^\pm = \frac{\sum\limits_{j=1,2} E^{(j)} \pm p_z^{(j)}}{\sum\limits_{i \in \text{hfs}} E^{(i)} \pm p_z^{(i)}}, \tag{7}$$

are used in this analysis to disentangle direct, singly, and doubly resolved production. In their definition, the sum in the numerator is over the two jets, and the sum in the denominator is over all hadronic final state particles, thereby distilling the energy-fraction the jets have w.r.t. the overall photon energies.

This is exemplified by, *e.g.*, the distribution of events in

$$\cos\Theta^* = \tanh\frac{\eta_1 - \eta_2}{2}, \tag{8}$$

an approximation of the angle between the two jets, and exhibited in Fig. 2. Apart from satisfying agreement with data, a few things are worth noticing here, which we will continue to observe also in the following: For $x_\gamma^\pm > 0.75$

the direct component dominates by about 1.5 orders of magnitude, with only small scale uncertainties, indicated by the pink band. Conversely, for $x_\gamma^\pm < 0.75$ the doubly-resolved component dominates with a significantly larger scale uncertainty, which, in this case, also includes factorization scale uncertainties. Intuitively, the singly-resolved component in both case ranges between the two other components. In addition we observe that hadronization effects reduce the cross section in the unresolved domanin, while the combination of hadronization and multiple parton scattering increases it in the doubly-resolved regime. The visible effect in the latter suggests that a careful retuning of the MPIs may further improve agreement with data.

We report that distributions in $x_\gamma^\pm$ for three different average di-jet transverse energies $\bar{E}_T = \sum_{j=1,2} E_T^{(j)}/2$ experience a significant improvement in shape when going from Leading to Next-to-Leading Order, *cf.* Fig. 3. However, in the transition region between doubly resolved to unresolved events, we notice a clear difference in shape: While for $x_\gamma^\pm < 0.6 - 0.7$ the prediction is relatively flat below the data, the underprediction at around $x_\gamma^\pm \approx 0.8$ persists at NLO. Apart from possibly insufficient photon PDFs – a point we will elucidate below – there are a number of possible explanations: First of all, as before, a retuning of MPIs may come to the rescue and fill up the gap.

Secondly, this drop around $x_\gamma^\pm \approx 0.7$ could be attributed to the missing QED splitting kernel in the evolution of the parton shower. Including this term would impact the backwards evolution of the photonic initial state radiation leading to a photon being reconstructed as the initial state also in the case of a resolved process. This again would lead to fewer radiation being generated, therefore shifting the distribution of the resolved process towards larger $x_\gamma^\pm$ values. The inclusion of this term in the evolution of the initial state showering is left for future work. Finally, we should stress that our singly resolved events are described by the $2 \to 2$ scat-

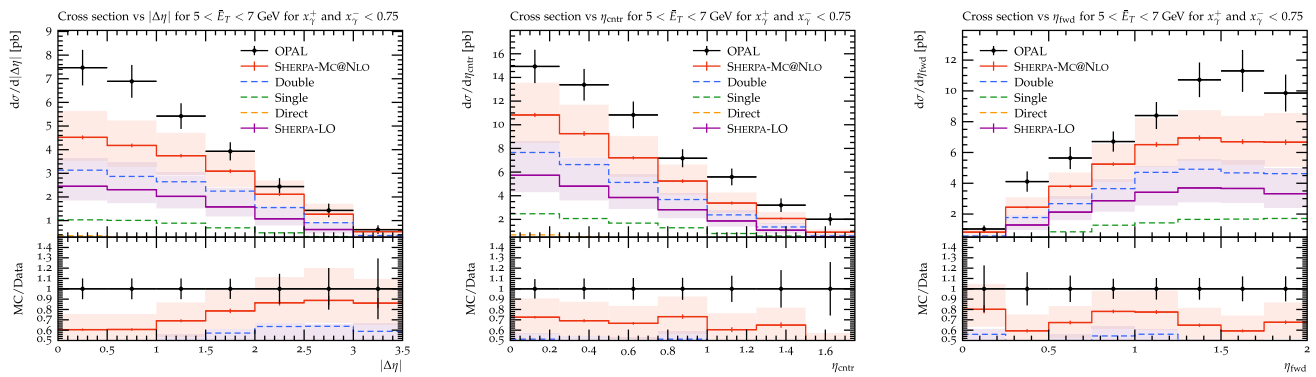**Fig. 4** Distributions of $|\Delta\eta|$ (left), $|\eta_{cntr}|$ (middle), and $|\eta_{fwd}|$ (right), comparing MC@NLO and LO. Results of the SHERPA simulation are compared with results from OPAL at an e^-e^+ c.m.-energy of 198 GeV [5]
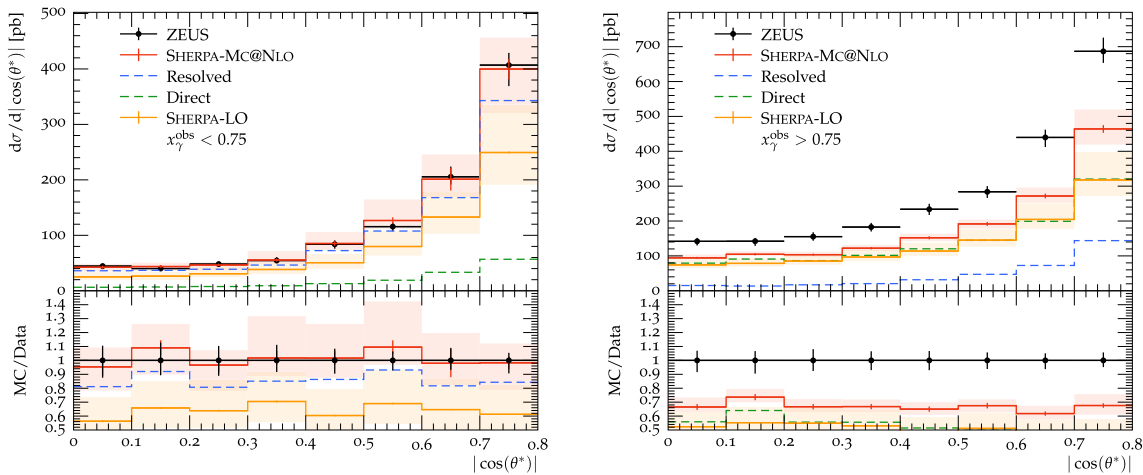

Fig. 5 Differential dijet inclusive cross section with respect to $\cos\theta^*$ for $x_\gamma^{obs} < 0.75$ (left) and $x_\gamma^{obs} > 0.75$ (right), comparing results of our SHERPA MC@NLO simulation with ZEUS Run-1 data [11]

tering of on-shell photons with partons from the resolved photons, an approximation which is probably not entirely correct as virtual photons would lead to a DIS-like scattering of the resolved photon, thereby inducing a somewhat different kinematics and scale choices.

Figure 4 shows distributions of jet pseudo-rapidities and their differences. Again, the overall shape of the prediction is improved and the lowered NLO cross-section is countered by the inclusion of Multiple-Parton Interactions (MPIs).

3.2 Comparison with HERA data

For the further validation of our implementation in electron–proton collisions we mainly rely on ZEUS data [12] taken at HERA Run 2. The kinematic cuts on the final states in the hard matrix element calculation were chosen to be a minimal transverse momentum of $p_T > 11(8)$ GeV for the (sub-)leading jets using the k_T clustering algorithm with radius $R = 1.0$ to safely capture the phase space cuts of $p_T^{(1)} > 14$ GeV and $p_T^{(2)} > 11$ GeV used in the analysis of the ZEUS

Run-1 data [11], even after taking into account MPIs. For the ZEUS Run-2 data [12], we chose $p_T > 13$ GeV to comply with the experimental cut of $E_T > 17$ GeV on the leading jet, with otherwise same settings.

We use the same scale setting algorithm as before, and we also evaluate the theory uncertainties as combination of scale and PDF uncertainties like in the case of electron–positron colliders in the section above. Defining, in analogy to the case at lepton colliders above, Eqs. (7) and (8), respectively,

$$x_\gamma^{obs} = \frac{E_T^{(1)} e^{-\eta^{(1)}} + E_T^{(2)} e^{-\eta^{(2)}}}{2y E_e} \quad \text{and}$$

$$\cos\theta^* = \tanh\frac{\eta^{(1)} - \eta^{(2)}}{2}. \tag{9}$$

Here $^{(1,2)}$ labels the leading and sub-leading jet, E_e is the lepton energy, and y is the energy fraction of the photon w.r.t. the lepton. As before we observe that the x_γ is excellently suited to disentangle unresolved and resolved photon interactions, *cf.* Fig. 5. In the resolved regime we again observe satisfactory agreement with data, indicating that the summa-
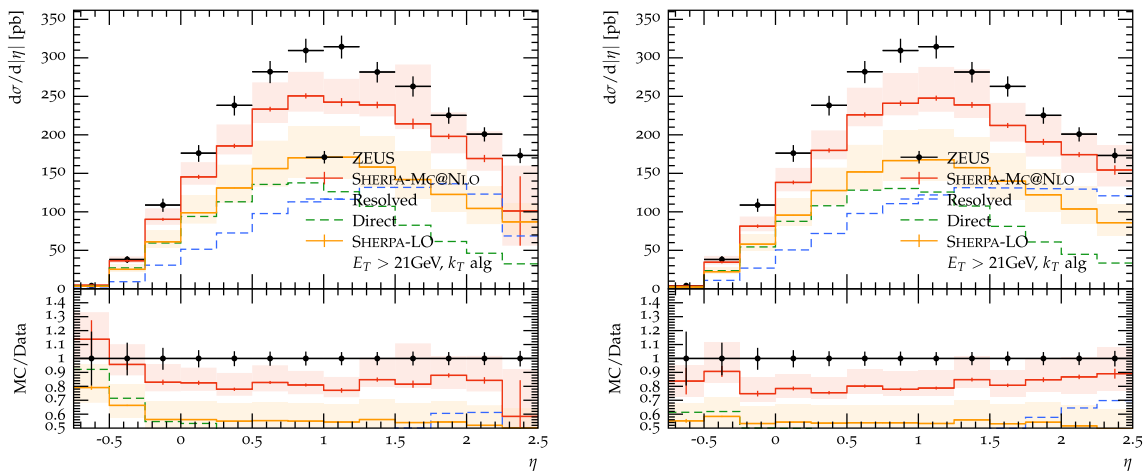
Fig. 6 Differential single-jet inclusive photo-production cross section with respect to the pseudo-rapidity of the leading jet, $\frac{d\sigma}{d\eta}$, comparing results of our SHERPA simulation at parton (left) and hadron-level (right) with ZEUS Run-2 data [12]
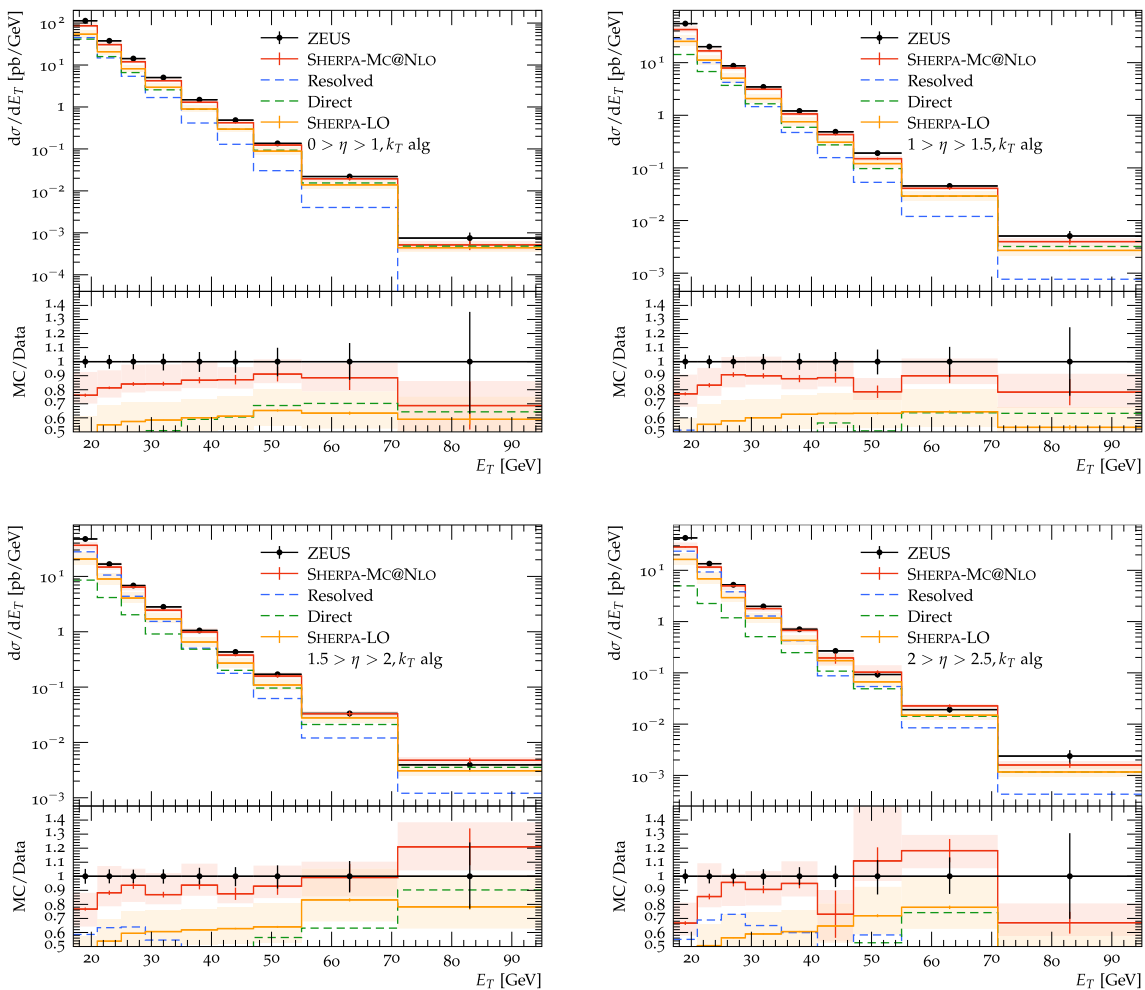

Fig. 7 Single-jet inclusive transverse energy spectra for the leading jet in different pseudo-rapidity bins of the k_T-jets: $0 < \eta < 1$ (top left), $1 < \eta < 1.5$ (top right), $1.5 < \eta < 2$ (bottom left), and $2 < \eta < 2.5$ (bottom right), comparing SHERPA MC@NLO results with ZEUS Run 2 data [12]
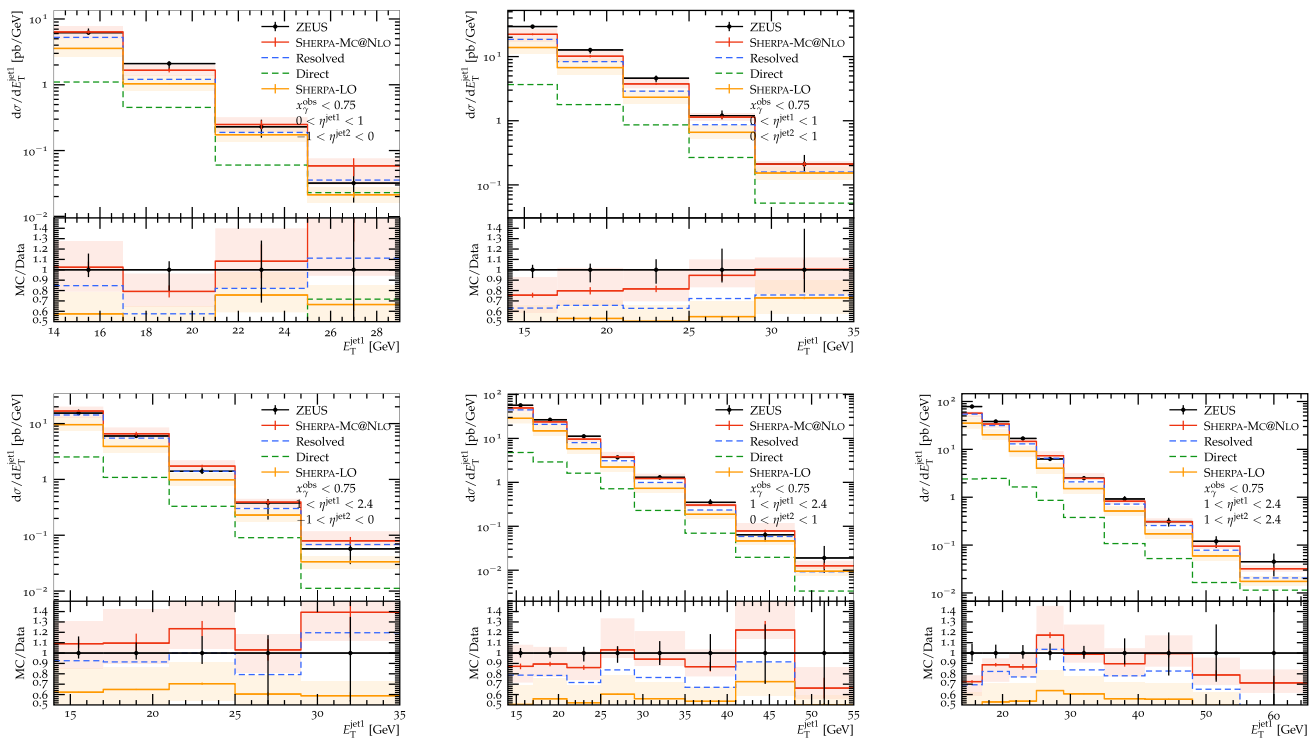
Fig. 8 Differential dijet inclusive cross section with respect to the transverse momentum of the leading jet, with $0 < \eta^{(1)} < 1$ (upper panel) and $1 < \eta^{(1)} < 2.4$ (lower panel) and in different bins for $\eta^{(2)}$, comparing results of our SHERPA MC@NLO simulation at hadron-level incl. MPI effects with the LO simulation and with data [11] taken by ZEUS at HERA Run 1

tion over the different components is correct. Interestingly, as suggested by the right panel of the figure, it appears as if the direct component is not sufficient to fully recover the experimental cross section. Possible explanations, as before, are related to the missing "anomalous" $\gamma \to q\bar{q}$ splitting in the backwards evolution, or, possibly more relevant here, a failure of the strictly on-shell approximation of the incident photons inherent to the treatment through EPA.

With this caveat in mind we will now turn into a more differential analysis of QCD final states in photo-production at HERA. In Fig. 6 we compare the parton- against the hadron-level results and as previously observed, the shape improves significantly through the combined effect of hadronization and MPIs. This is most visible in the phase space of $\eta < 0$, rendering the distribution of the simulation data flat compared to the experimental data. While there remains a discrepancy between simulation and data of around 10-20%, it might be explained by three observations. First, this analysis cuts requires only one jet in the final state which allows for contributions from the DIS region to leak into this measurement, for example if the scattered beam electron has not been correctly detected or identified. Secondly, the precise value of the strong coupling in the fit of the photon PDFs is not explicitly mentioned in the corresponding publications [22,23]. An updated photon PDF fit would be performed with

the current world average of α_S and might further reduce the discrepancy. Lastly, the modelling of multiple-parton interactions for photon–proton interactions needs a fitting to the data for both proton–proton and photon–proton data. As neither have been tuned to data yet it can be suspected that the MPI will receive larger contributions, thereby improving overall agreement of simulation and data.

The spectrum of the jet transverse energies E_T, displayed in Fig. 7 exhibits a slight shape in the distribution for forward jets and small E_T. The same effect can be seen in Fig. 8, where the simulation describes data well for central leading jets, but worsens as both go more forward. As this part of the phase receives contributions from the MPIs, we again suspect that the naive parameter choice underestimate the amount of additionally generated radiation.

3.3 Photon PDF for precision phenomenology

The predictions of photo-production cross sections and distributions in low-x_γ space exhibit large variations depending on the used photon PDF. In fact, these deviations can be as large or even larger in value than the estimate of higher-order corrections through the scale variations, especially for the simulation of photo-production at lepton colliders, see Fig. 9. There we show the very inclusive $\cos\Theta^*$ and $\cos\theta^*$
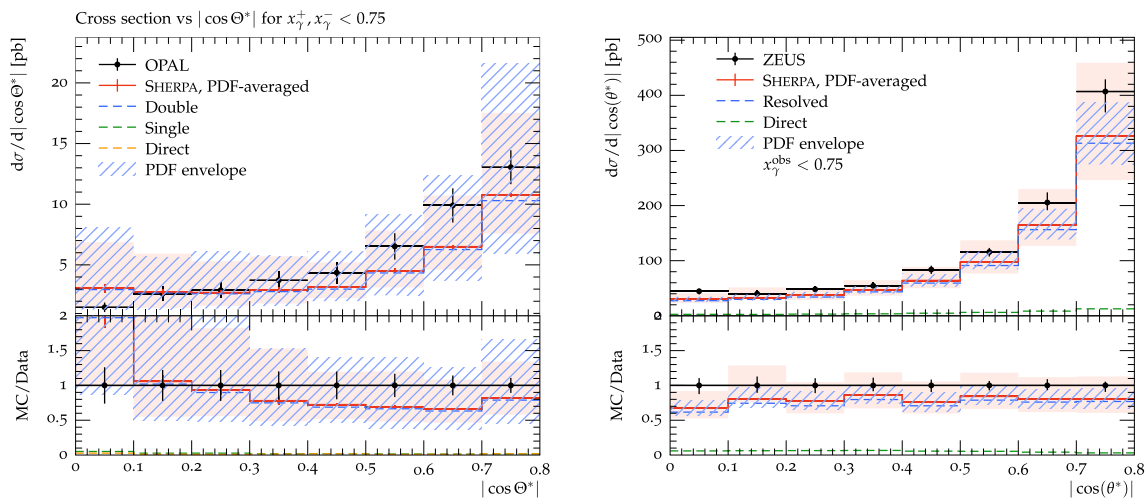
Fig. 9 Distributions for cos Θ^* at LEP (left) and for cos θ^* at HERA (right), comparing SHERPA's LO simulations with data from OPAL [5] and ZEUS [11]. Scale uncertainties at LO are indicated by the pink band, while PDF uncertainties are shown with the blue hatched area

Table 2 Inclusive cross-sections for one million events in a HERA Run 1 dijet photo-production setup with two different proton PDFs and the same PDF for the photon

PDF	NNPDF23_lo_as_0130_qed [61]	PDF4LHC21_40_pdfas [62]
α_S	0.13	0.118
Order	1	3
$\sigma(\gamma j \to jj)$ / nb	2.85 ± 0.02	2.303 ± 0.016
$\sigma(jj \to jj)$ / nb	2.151 ± 0.002	1.997 ± 0.002

distributions, obtained at leading order, at LEP and HERA, respectively., indicating LO scale and PDF uncertainties separately. For the latter we present the full range of results from all available leading order PDFs, and we observe that the PDF uncertainties alone are of equal size as the LO scale uncertainties. This underlines the need for a comprehensive retuning of the photon PDFs with available data, and including higher-order calculations and simulations.

It is also worth noting that a consistent simulation of photo-production at hadron–lepton colliders necessitates a combined fit of the photon and proton PDFs. Depending on the proton PDF and its value for α_S the inclusive cross-section in a HERA Run 2 simulation gives deviations of about 20%, as can be seen in Tab. 2. This underlines the necessity for a systematic refit of photon PDFs to use in conjunction with modern proton PDFs. While no new data has been taken since the retiring of the HERA collider, a consistent fit to all the data with the updated values for α_S and including error estimates should increase the confidence in precision phenomenology for photo-production for the planned EIC and other future colliders.

4 Summary

In this paper we reported on developments of the SHERPA event generator towards the first hadron-level simulation of photo-production at NLO accuracy, to be published in our upcoming SHERPA 3.0 public release. We described how the initial state phase space is treated to allow for a flexible yet efficient integration of different spectra and distributions, based on the equivalent photon approximation and the inclusion of a broad range of photon PDFs. We validated our model by comparison to data from the LEP and HERA experiments and found satisfactory agreement between the data and the simulation, noting that the non-perturbative aspects of the simulation, in particular intrinsic k_T and multiple-parton interactions, still require a comprehensive tuning to data. Apart from possible improvement in this sector of the simulation, our analysis of uncertainties underlined the necessity for a refitting of the photon PDFs, especially in view of the anticipated precision of the planned electron-ion collider. We believe that this step – a first refitting of photon PDFs after 20 years – based on higher-order calculations, modern sim-

ulation tools at least at NLO accuracy, and recent proton PDFs will siginifcantly improve the quality of our theoretical preprations for this new collider experiment.

Data availability statement This manuscript has no associated data or the data will not be deposited. [Authors' comment: The code to reproduce the plots will be made public in the forthcoming Sherpa release.]

References

1. J.P. Lees et al., Measurement of the $\gamma^\star\gamma^\star \to \eta'$ transition form factor. Phys. Rev. D **98**(11), 112002 (2018). https://doi.org/10.1103/PhysRevD.98.112002. arXiv:1808.08038 [hep-ex]

2. Ragoni, S.: New measurements on diffractive vector mesons. PoS LHCP2021, 085 (2021). https://doi.org/10.22323/1.397.0085. arXiv:2109.03066 [hep-ex]

3. Klein, S.R.: ρ photoproduction in ALICE. In: Low-x Workshop 2021 (2021)

4. Tu, Z.: Exclusive J/ photoproduction off deuteron in d+Au ultra-peripheral collisions at STAR. PoS HardProbes2020, 100 (2021). https://doi.org/10.22323/1.387.0100. arXiv:2009.04860 [nucl-ex]

5. G. Abbiendi et al., Dijet production in photon-photon collisions at s(ee)**(1/2) from 189-GeV to 209-GeV. Eur. Phys. J. C **31**, 307–325 (2003). https://doi.org/10.1140/epjc/s2003-01360-8. arXiv:hep-ex/0301013

6. G. Abbiendi et al., Inclusive Jet Production in Photon-Photon Collisions at s(ee)**(1/2) from 189 to 209-GeV. Phys. Lett. B **658**, 185–192 (2008). https://doi.org/10.1016/j.physletb.2007.08.096. arXiv:0706.4382 [hep-ex]

7. P. Achard et al., Inclusive jet production in two-photon collisions at LEP. Phys. Lett. B **602**, 157–166 (2004). https://doi.org/10.1016/j.physletb.2004.10.003. arXiv:hep-ex/0410012

8. G. Abbiendi et al., Total hadronic cross-section of photon-photon interactions at LEP. Eur. Phys. J. C **14**, 199–212 (2000). https://doi.org/10.1007/s100520000352. arXiv:hep-ex/9906039

9. K. Ackerstaff et al., Inclusive production of charged hadrons and K0(S) mesons in photon-photon collisions. Eur. Phys. J. C **6**, 253–264 (1999). https://doi.org/10.1007/s100529801028. arXiv:hep-ex/9808009

10. G. Abbiendi et al., Inclusive production of D*+- mesons in photon-photon collisions at S**(1/2)(ee) = 183-GeV and 189-GeV and a first measurement of F**gamma(2, c). Eur. Phys. J. C **16**, 579–596 (2000). https://doi.org/10.1007/s100520000420. arXiv:hep-ex/9911030

11. S. Chekanov et al., Dijet photoproduction at HERA and the structure of the photon. Eur. Phys. J. C **23**, 615–631 (2002). https://doi.org/10.1007/s100520200936. arXiv:hep-ex/0112029

12. H. Abramowicz et al., Inclusive-jet photoproduction at HERA and determination of alphas. Nucl. Phys. B **864**, 1–37 (2012). https://doi.org/10.1016/j.nuclphysb.2012.06.006. arXiv:1205.6153 [hep-ex]

13. M. Derrick et al., Measurement of the F2 structure function in deep inelastic e+ p scattering using 1994 data from the ZEUS detector at HERA. Z. Phys. C **72**, 399–424 (1996). https://doi.org/10.1007/s002880050260. arXiv:hep-ex/9607002

14. J. Breitweg et al., ZEUS results on the measurement and phenomenology of F(2) at low x and low Q**2. Eur. Phys. J. C **7**, 609–630 (1999). https://doi.org/10.1007/s100529901084. arXiv:hep-ex/9809005

15. S. Chekanov et al., Exclusive photoproduction of J / psi mesons at HERA. Eur. Phys. J. C **24**, 345–360 (2002). https://doi.org/10.1007/s10052-002-0953-7. arXiv:hep-ex/0201043

16. C. Adloff et al., Measurement and QCD analysis of neutral and charged current cross-sections at HERA. Eur. Phys. J. C **30**, 1–32 (2003). https://doi.org/10.1140/epjc/s2003-01257-6. arXiv:hep-ex/0304003

17. C. Adloff et al., Elastic photoproduction of J / psi and Upsilon mesons at HERA. Phys. Lett. B **483**, 23–35 (2000). https://doi.org/10.1016/S0370-2693(00)00530-X. arXiv:hep-ex/0003020

18. M. Glück, E. Reya, A. Vogt, Photonic parton distributions. Phys. Rev. D **46**(5), 1973–1979 (1992). https://doi.org/10.1103/physrevd.46.1973

19. F. Cornet, P. Jankowski, M. Krawczyk, A. Lorca, A New five flavor LO analysis and parametrization of parton distributions in the real photon. Phys. Rev. D **68**, 014010 (2003). https://doi.org/10.1103/PhysRevD.68.014010. arXiv:hep-ph/0212160

20. F. Cornet, P. Jankowski, M. Krawczyk, A New 5 flavor NLO analysis and parametrizations of parton distributions of the real photon. Phys. Rev. D **70**, 093004 (2004). https://doi.org/10.1103/PhysRevD.70.093004. arXiv:hep-ph/0404063

21. Slominski, W., Abramowicz, H., Levy, A.: NLO photon parton parametrization using ee and ep data. Eur. Phys. J. C **45**, 633–641 (2006). https://doi.org/10.1140/epjc/s2005-02458-7. arXiv:hep-ph/0504003

22. G.A. Schuler, T. Sjöstrand, Low- and high-mass components of the photon distribution functions. Zeitschrift für Physik C Particles and Fields **68**(4), 607–623 (1995). https://doi.org/10.1007/bf01565260. arXiv:hep-ph/9503384

23. Schuler, G.A., Sjöstrand, T.: Parton Distributions of the Virtual Photon. Phys. Lett. B **376**, 193–200 (1996). https://doi.org/10.1016/0370-2693(96)00265-1. arXiv:hep-ph/9601282

24. G.A. Schuler, T. Sjöstrand, A scenario for high-energy $\gamma\gamma$ interactions. Z. Phys. C **73**, 677–688 (1997). https://doi.org/10.1007/s002880050359. arXiv:hep-ph/9605240

25. Sjöstrand, T., Mrenna, S., Skands, P.: PYTHIA 6.4 physics and manual. JHEP **05**, 026 (2006) arXiv:hep-ph/0603175

26. Bierlich, C., et al.: A comprehensive guide to the physics and usage of PYTHIA 8.3. SciPost Phys. Codebases (2022). https://doi.org/10.21468/SciPostPhysCodeb.8. arXiv:2203.11601 [hep-ph]

27. M. Klasen, G. Kramer, Inclusive two jet production at HERA: Direct and resolved cross-sections in next-to-leading order QCD. Z. Phys. C **76**, 67–74 (1997). https://doi.org/10.1007/s002880050528. arXiv:hep-ph/9611450

28. S. Frixione, G. Ridolfi, Jet photoproduction at HERA. Nucl. Phys. **B507**, 315–333 (1997). https://doi.org/10.1016/S0550-3213(97)00575-0. arXiv:hep-ph/9707345

29. G. Kramer, B. Pötter, Low Q^2 jet production at HERA in next-to-leading order QCD. Eur. Phys. J. C **5**, 665–679 (1998). https://doi.org/10.1007/s100520050308. arXiv:hep-ph/9804352

30. M. Klasen, T. Kleinwort, G. Kramer, Inclusive Jet Production in γp and $\gamma \gamma$ Processes: Direct and Resolved Photon Cross Sections in Next-To-Leading Order QCD. Eur. Phys. J. direct **1**(1), 1 (1998). https://doi.org/10.1007/s101059800001. arXiv:hep-ph/9712256

31. B.W. Harris, J.F. Owens, Photoproduction of jets at HERA in next-to-leading order QCD. Phys. Rev. D **56**, 4007–4016 (1997). https://doi.org/10.1103/PhysRevD.56.4007. arXiv:hep-ph/9704324

32. V. Guzey, M. Klasen, Inclusive and Diffractive Dijet Photoproduction at the Electron-Ion Collider in NLO QCD. Acta Phys. Polon. Supp. **16**(7), 7–11 (2023). https://doi.org/10.5506/APhysPolBSupp.16.7-A11. arXiv:2303.05182 [hep-ph]

33. C.-H. Chang, R. Li, J.-X. Wang, J/psi polarization in photoproduction up-to the next-to-leading order of QCD. Phys. Rev. D **80**, 034020 (2009). https://doi.org/10.1103/PhysRevD.80.034020. arXiv:0901.4749 [hep-ph]

34. K.J. Eskola, C.A. Flett, V. Guzey, T. Löytäinen, H. Paukkunen, Exclusive J/ψ photoproduction in ultraperipheral Pb+Pb collisions at the CERN Large Hadron Collider calculated at next-to-leading order perturbative QCD. Phys. Rev. C **106**(3), 035202 (2022). https://doi.org/10.1103/PhysRevC.106.035202. arXiv:2203.11613 [hep-ph]

35. K.J. Eskola, C.A. Flett, V. Guzey, T. Löytäinen, H. Paukkunen, Next-to-leading order perturbative QCD predictions for exclusive J/ψ photoproduction in oxygen-oxygen and lead-lead collisions at energies available at the CERN Large Hadron Collider. Phys. Rev. C **107**(4), 044912 (2023). arXiv:2210.16048 [hep-ph]

36. K.J. Eskola, C.A. Flett, V. Guzey, T. Löytäinen, H. Paukkunen, Predictions for exclusive Υ photoproduction in ultraperipheral Pb+Pb collisions at the LHC at next-to-leading order in perturbative QCD. Eur. Phys. J. C **83**(8), 758 (2023). https://doi.org/10.1140/epjc/s10052-023-11927-8. arXiv:2303.03007 [hep-ph]

37. S.P. Jones, A.D. Martin, M.G. Ryskin, T. Teubner, Exclusive J/ψ and Υ photoproduction and the low x gluon. J. Phys. G **43**(3), 035002 (2016). https://doi.org/10.1088/0954-3899/43/3/035002. arXiv:1507.06942 [hep-ph]

38. Jones, S.P., Martin, A.D., Ryskin, M.G., Teubner, T.: Probes of the small x gluon via exclusive J/ψ and Υ production at HERA and the LHC. JHEP **11**, 085 (2013). https://doi.org/10.1007/JHEP11(2013)085. arXiv:1307.7099 [hep-ph]

39. Gleisberg, T., Höche, S., Krauss, F., Schönherr, M., Schumann, S., Siegert, F., Winter, J.: Event generation with SHERPA 1.1. JHEP **02**, 007 (2009). https://doi.org/10.1088/1126-6708/2009/02/007. arXiv:0811.4622 [hep-ph]

40. E. Bothmann et al., Event Generation with Sherpa 2.2. SciPost Phys **7**(3), 034 (2019). https://doi.org/10.21468/SciPostPhys.7.3.034. arXiv:1905.09127 [hep-ph]

41. R. Kleiss, R. Pittau, Weight optimization in multichannel Monte Carlo. Comput. Phys. Commun. **83**, 141–146 (1994). https://doi.org/10.1016/0010-4655(94)90043-4. arXiv:hep-ph/9405257

42. C.F. Weizsäcker, Radiation emitted in collisions of very fast electrons. Z.Phys **88**, 612–625 (1934). https://doi.org/10.1007/BF01333110

43. E.J. Williams, Nature of the high-energy particles of penetrating radiation and status of ionization and radiation formulae. Phys. Rev. **45**, 729–730 (1934). https://doi.org/10.1103/PhysRev.45.729

44. Budnev, V.M., Ginzburg, I.F., Meledin, G.V., Serbo, V.G.: The two photon particle production mechanism. Physical problems. Applications. Equivalent photon approximation. Phys. Rept. **15**, 181–281 (1974)

45. S. Frixione, M.L. Mangano, P. Nason, G. Ridolfi, Improving the Weizsacker-Williams approximation in electron - proton collisions. Phys. Lett. B **319**, 339–345 (1993)

46. collaboration, S.: Sherpa Project webpage. https://sherpa-team.gitlab.io/. Accessed: 24 Jan 2024

47. S. Frixione, M.L. Mangano, P. Nason, G. Ridolfi, Heavy quark production. Adv. Ser. Direct. High Energy Phys. **15**, 609–706 (1998). https://doi.org/10.1142/9789812812667_0009. arXiv:hep-ph/9702287

48. S. Catani, M.H. Seymour, A general algorithm for calculating jet cross sections in NLO QCD. Nucl. Phys. B **485**, 291–419 (1997). arXiv:hep-ph/9605323

49. Krauss, F., Kuhn, R., Soff, G.: AMEGIC++ 1.0: A Matrix Element Generator In C++. JHEP 02, 044 (2002) arXiv:hep-ph/0109036

50. T. Gleisberg, S. Höche, Comix, a new matrix element generator. JHEP **12**, 039 (2008). https://doi.org/10.1088/1126-6708/2008/12/039. arXiv:0808.3674 [hep-ph]

51. T. Gleisberg, F. Krauss, Automating dipole subtraction for QCD NLO calculations. Eur. Phys. J. C **53**, 501–523 (2008). arXiv:0709.2881 [hep-ph]

52. F. Buccioni, J.-N. Lang, J.M. Lindert, P. Maierhöfer, S. Pozzorini, H. Zhang, M.F. Zoller, OpenLoops 2. Eur. Phys. J. C **79**(10), 866 (2019). https://doi.org/10.1140/epjc/s10052-019-7306-2. arXiv:1907.13071 [hep-ph]

53. Schumann, S., Krauss, F.: A parton shower algorithm based on Catani-Seymour dipole factorisation. JHEP **03**, 038 (2008). arXiv:0709.1027 [hep-ph]

54. S. Frixione, B.R. Webber, Matching NLO QCD computations and parton shower simulations. JHEP **06**, 029 (2002). arXiv:hep-ph/0204244

55. S. Frixione, P. Nason, B.R. Webber, Matching NLO QCD and parton showers in heavy flavour production. JHEP **08**, 007 (2003). arXiv:hep-ph/0305252

56. S. Höche, F. Krauss, M. Schönherr, F. Siegert, A critical appraisal of NLO+PS matching methods. JHEP **09**, 049 (2012). arXiv:1111.1220 [hep-ph]

57. T. Sjöstrand, M. Zijl, A multiple-interaction model for the event structure in hadron collisions. Phys. Rev. D **36**, 2019 (1987)

58. G.A. Schuler, T. Sjostrand, Hadronic diffractive cross-sections and the rise of the total cross-section. Phys. Rev. D **49**, 2257–2267 (1994)

59. G.S. Chahal, F. Krauss, Cluster hadronisation in sherpa. SciPost Phys. **13**(2), 019 (2022). https://doi.org/10.21468/SciPostPhys.13.2.019. arXiv:2203.11385 [hep-ph]

60. C. Bierlich et al., Robust independent validation of experiment and theory: Rivet version 3. SciPost Phys. **8**, 026 (2020). https://doi.org/10.21468/SciPostPhys.8.2.026. arXiv:1912.05451 [hep-ph]

61. R.D. Ball et al., Parton distributions with LHC data. Nucl. Phys. B **867**, 244–289 (2013). https://doi.org/10.1016/j.nuclphysb.2012.10.003. arXiv:1207.1303 [hep-ph]

62. R.D. Ball et al., The PDF4LHC21 combination of global PDF fits for the LHC Run III. J. Phys. G **49**(8), 080501 (2022). https://doi.org/10.1088/1361-6471/ac7216. arXiv:2203.05506